Computers and Structures 87 (2009) 604–617

Contents lists available at ScienceDirect

Computers and Structures

journal homepage: www.elsevier.com/locate/compstruc

A mesh adaptivity procedure for CFD and fluid-structure interactions

Klaus-Jürgen Bathe [a,*], Hou Zhang [b]

[a] Massachusetts Institute of Technology, Cambridge, MA, USA
[b] ADINA R&D, Inc., Watertown, MA, USA

ARTICLE INFO

Article history:
Received 7 January 2009
Accepted 28 January 2009
Available online 1 April 2009

Keywords:
CFD
Fluid-structure interaction, FSI
Large structural deformations
Mesh adaptivity
Mesh repair

ABSTRACT

We present a procedure to adapt and repair meshes in the general solution of Navier–Stokes incompressible and compressible fluid flows, including structural interactions. For fluid-structure interactions, FSI, the fluid is described by an arbitrary-Lagrangian–Eulerian formulation fully coupled to general solids and structures described by Lagrangian formulations. The solids and structures can undergo highly nonlinear response due to large deformations, nonlinear material behavior, contact and temperature. We focus on the need to adapt the fluid mesh in pure CFD solutions when high gradients are present or boundary layer effects are important, and FSI solutions when large structural deformations take place. The procedure is a practical scheme to solve complex problems. We illustrate the proposed scheme in various example solutions.

© 2009 Elsevier Ltd. All rights reserved.

1. Introduction

The solution of fluid-structure interactions, FSI, with computational fluid dynamics, CFD, has been given increased attention during the recent years [1,2]. This is largely because finite element and finite volume methods, including the equation solvers, have become very powerful and can frequently be used at reasonable costs in scientific and engineering studies. We consider in this paper incompressible and compressible fluids and very general solids and structures.

In essence, there are two approaches for the solution of fluid-structure interactions. In the first approach, an arbitrary-Lagrangian–Eulerian formulation is employed for the fluid and a Lagrangian formulation for the solid or structure [1,2]. This approach is mostly employed, and monolithic and partitioned simulations are performed [3]. In the second approach, an Eulerian formulation is used for the fluid, with a stationary fluid mesh, and a Lagrangian formulation is used for the structure [1,2]. In these solutions, the Lagrangian mesh of the solid moves through the fluid mesh. The formulations used are referred to as immersed methods. This approach is now largely in the research stage, because a number of limitations are still present, but has much potential. Of course, the formulations and numerical techniques used in these approaches can also be combined.

There are numerous important applications where the fluid flow must be predicted accurately. When three-dimensional (3D) flows need be simulated, the computational effort can become large and efficient meshes are best used. Therefore mesh grading is required. However, the optimal grading depends on the fluid flow, that is, on the solution. Hence effective procedures that iteratively adapt the mesh dependent on the solution are very desirable.

There are also numerous applications where fluid flows are fully coupled to the response of structures. While many such problems can now be solved already using an arbitrary-Lagrangian–Eulerian formulation [1,2], the major shortcoming is that when the structure undergoes large deformations, the fluid mesh may get highly distorted. Indeed, the mesh may become so distorted that the solution cannot be continued, unless the mesh is repaired or iteratively adapted.

In engineering practice and scientific studies, it is clearly best to have one solution capability that is sufficiently general to solve complex CFD and FSI problems. These problems may contain incompressible (including slightly compressible) flows or compressible (including low-speed compressible) flows. Considering fluid structure interactions, the structure, or solid, may be quite flexible in membrane or shell behavior. Hence the structural deformations can be complex and be highly affected by the specific flow that takes place. Of course, the fluid flow can also be highly affected by the structural deformations [1–4]. In all cases, the aim is in general to obtain, at a reasonable cost, sufficiently accurate predictions of the fluid and structural response.

Our objective in this paper is to present some developments to establish automatically graded meshes that are effective in CFD and FSI analyses. We assume that the fluid flow is governed by the Navier–Stokes equations, hence we do not consider acoustic fluids governed by displacement or potential formulations, see,

* Corresponding author. Tel.: +1 617 253 6645.
E-mail address: kjb@mit.edu (K.J. Bathe).

0045-7949/$ - see front matter © 2009 Elsevier Ltd. All rights reserved.
doi:10.1016/j.compstruc.2009.01.017

Table 1
Operations on criteria for element size selection.

Operation	Definition	Note	
Append	$E \cup (E_i \setminus E)$	Append E_i to E	
Replace	$E_i \cup (E \setminus E_i)$	Append E to E_i	
Subtract	$E \setminus E_i$	Subtract E_i from E	
Smaller		Join E and E_i and	$h_{ep} =: \min\{h_{ep}, h_{epi}\}$
Larger	$(E \setminus E_i) \cup (E_i \setminus E) \cup (E \cap E_i)$	update h_{ep} if	$h_{ep} =: \max\{h_{ep}, h_{epi}\}$
Average		$e \in E \cap E_i$	$h_{ep} =: \frac{1}{2}(h_{ep} + h_{epi})$

e.g. [2,5–7]. The procedures we present are directed to usage in engineering and the sciences to solve complex viscous fluid flows that may contain structural interactions.

In Sections 2–4, we first consider incompressible flows and comment on the flow-condition-based finite elements that we use to solve the incompressible (or slightly compressible) Navier–Stokes equations, including turbulence models. We then summarize our approach to solve the compressible Navier–Stokes equations. For FSI simulations, the discretization schemes for incompressible and compressible flows are used in the same manner with an arbitrary-Lagrangian–Eulerian formulation that is coupled to the Lagrangian formulations of solids and structures [4,8,9]. All finite element formulations including contact conditions are described elsewhere [4,10–13], where it is important to note that the solids and structures can undergo very large deformations. When large structural deformations occur, the solution of an FSI problem can represent a particular challenge [4,14].

In Section 5, we then present the specific procedures that we use to repair and adapt meshes in order to obtain effective CFD and FSI solutions. These techniques operate on solution gradients and involve adapting (that is, refining and coarsening) the mesh to have adequate element sizes throughout the fluid region.

To demonstrate the use of the solution schemes, we present in Section 6 some illustrative example solutions, and finally, in Section 7, we give our concluding remarks.

2. Incompressible fluid flows

In this section we comment on the discretization methods that we use for the solution of the incompressible Navier–Stokes equations. We use the flow-condition-based interpolation (FCBI) approach that we developed with two specific aims in mind [4,11].

Firstly, the solution of the Navier–Stokes equations should be stable and reasonably accurate with a rather coarse mesh [4,15]. If the mesh is fine, of course, an accurate solution should be obtained, but also, *a reasonable coarse mesh should result in a reasonable solution*. We want this property of the discretization scheme because the coarse mesh provides a starting solution from which we can iterate towards a more refined mesh to obtain an accurate solution. This property is of particular value when considering FSI solutions, as we further discuss and illustrate below. We also want this property because, for certain types of flows the local Reynolds number of flow is usually not known prior to the solution, and hence it may not be clear whether to use a turbulence model. Once insight into the flow has been obtained through a coarse mesh solution, an appropriate turbulence model could be used.

Secondly, the FCBI formulation satisfies local conservation of mass and momentum, and is used without adjusting numerical factors [4,11,16]. The elements can be employed for low and high Reynolds number flows with the interpolation functions adjusting automatically to the specific flow conditions to provide stability of the solutions. Of course, the FCBI formulation approach can also be combined with other approaches to possibly find more effective solution strategies, see, e.g. [17].

Considering general incompressible, slightly compressible and low-speed compressible fluid flows, the governing equations are the conservation of mass, momentum and energy [10,18]:

$$\frac{\partial \rho}{\partial t} + \nabla \cdot (\rho \mathbf{v}) = 0, \tag{1}$$

$$\frac{\partial \rho \mathbf{v}}{\partial t} + \nabla \cdot (\rho \mathbf{v}\mathbf{v} - \boldsymbol{\tau}) = \mathbf{f}^B, \tag{2}$$

$$c_v \left[\frac{\partial \rho \theta}{\partial t} + \nabla \cdot (\rho \mathbf{v} \theta) \right] + \nabla \cdot \mathbf{q} = q^B, \tag{3}$$

where

$$\boldsymbol{\tau} = -p\mathbf{I} + \mu[\nabla \mathbf{v} + (\nabla \mathbf{v})^T)], \tag{4}$$

$$\mathbf{q} = -k \nabla \theta \tag{5}$$

with appropriately prescribed boundary conditions on velocities, pressure, temperature, in-flows and out-flows, and so on.

In Eqs. (1)–(5), $\mathbf{v}$ is the velocity, p is the pressure, ρ is the density, $\boldsymbol{\tau}$ is the stress, θ is the temperature, t is the time, c_v is the specific heat at constant volume, $\mathbf{q}$ is the heat flux, μ is the

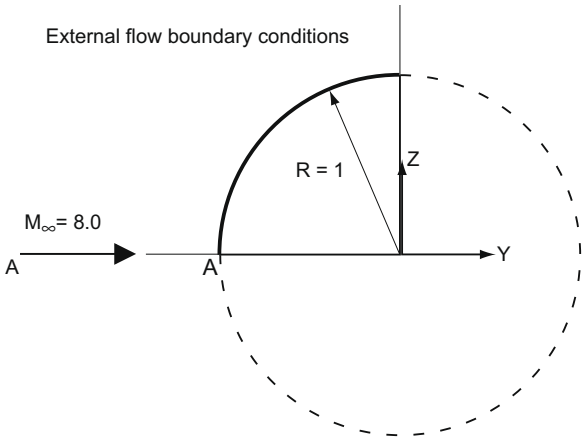

Fig. 1. Compressible planar flow passing a cylinder.

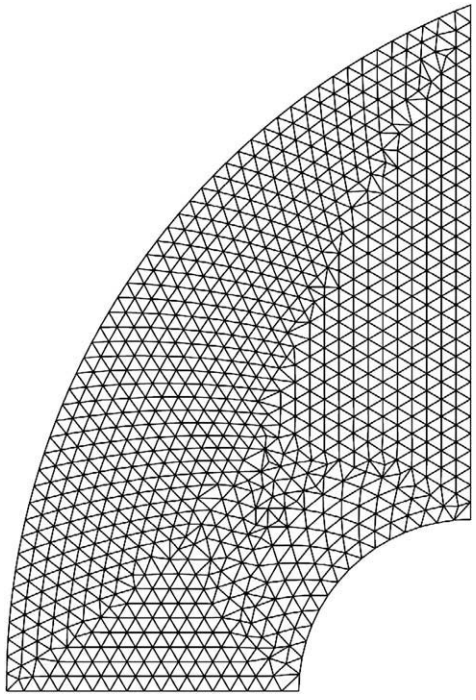

Fig. 2. Starting mesh for compressible flow passing a cylinder.

viscosity, k is the thermal conductivity, $\mathbf{f}^B$ is the body force per unit volume, and q^B is the rate of heat generated per unit volume.

As mentioned above, we use the flow-condition-based finite element approach to numerically solve these equations [4,11].

The basic equations (1)–(3) assume laminar flow. To introduce turbulence models, these equations are supplemented in a standard manner by the basic equations of the turbulence models. The solution of the transport equations governing the turbulence effects is then accomplished using the same numerical scheme.

3. High-speed compressible flows

The governing equations of high-speed compressible flows are in their strong conservation form

$$\frac{\partial \mathbf{U}}{\partial t} + \nabla \cdot \mathbf{F} = \mathbf{S} \tag{6}$$

with

$$\mathbf{U} = \begin{bmatrix} \rho \\ \rho \mathbf{v} \\ \rho E \end{bmatrix}, \quad \mathbf{F} = \begin{bmatrix} \rho \mathbf{v} \\ \rho \mathbf{v}\mathbf{v} - \boldsymbol{\tau} \\ \rho \mathbf{v} E - \boldsymbol{\tau} \cdot \mathbf{v} - k \nabla \theta \end{bmatrix}, \quad \mathbf{S} = \begin{bmatrix} 0 \\ \mathbf{f}^B \\ \mathbf{f}^B \cdot \mathbf{v} + q^B \end{bmatrix}, \tag{7}$$

where $E(=\frac{1}{2}\mathbf{v}\cdot\mathbf{v} + e)$ is the specific energy and e is the internal energy. These equations are subject to appropriate boundary conditions to model various flow conditions [8,18]. To solve these equations we use the Roe scheme proposed by Glaister [19] incorporated into our finite element procedure.

4. Solids and structures coupled to fluid flows

The above fluid equations are used in an arbitrary Lagrangian–Eulerian framework in the FSI solutions [4]. The structural domains are described using a Lagrangian formulation and can comprise solids, shells, beams, and other structural elements, including contact surfaces [10]. Of particular interest in fluid-structure interactions is the capability to analyze thin shells interacting with fluid flows. However, thin shell structures display a variety of deformation behaviors [20,21] and the analysis of their interactions with fluid flows can be a particular challenge.

The governing finite element equations fully coupling the fluid flow and structural response can be written as [4]

$$\mathbf{F}(\mathbf{X}) = \begin{bmatrix} \mathbf{F}_f(\mathbf{X}_f, \mathbf{X}_s) \\ \mathbf{F}_s(\mathbf{X}_f, \mathbf{X}_s) \end{bmatrix} = \mathbf{0}, \tag{8}$$

where, respectively, $\mathbf{F}_f$ and $\mathbf{F}_s$ represent the equation systems for the fluid and solid models, and $\mathbf{X}_f$ and $\mathbf{X}_s$ are the fluid and solid solution variables, including the displacements of the FSI interface. These equations hold for steady-state and transient solutions, where for transient analyses we use for the first-order fluid and second-order structural equations the 'consistent' time integration scheme of Ref. [22].

Eq. (8) contains all momentum, energy and continuity conditions of the fluid and solid, and all interface conditions between the fluid and the solid. With the algorithm we use, the patch tests involving the fluid and solid are passed [10,23]. The equations can be solved directly in monolithic form or iteratively in partitioned form. There are advantages to each approach depending on the problem considered and the computer available for solution [1–4,24].

5. Procedure for mesh adaptivity

The mesh adaptation procedure contains various ingredients that we discuss below. The procedure is based on the use of free-form meshing with 3-node triangular elements in 2D flows and 4-node tetrahedral elements in 3D flows.

5.1. Selection of element sizes

It is well known that the optimal element distribution for the computation of a numerical solution is, in essence, the one for which the local error is constant for all elements [10]. However, actual accurate error estimates in the numerical solution of highly nonlinear shell, CFD and FSI problems are either not yet available or expensive to calculate [21,25,26]. Hence, we base our mesh adaptation scheme on the well-known general fact that whatever field is to be predicted accurately, the element 'size' (with a length scale) times the gradient of that field should be about constant over the fluid region. The novelty in our scheme is how we specifically use various criteria.

In FSI solutions, we use in this paper the mesh adaptivity only for the fluid. For the solid or shell we simply use a sufficiently fine discretization because the major expense of solution pertains to the CFD mesh.

Specifically, for the CFD mesh, we use the local criterion C to choose element sizes

$$C(F_e): \quad h_{ep}\|F_e\| = c, \tag{9}$$

where c is a constant, h_{ep} is the locally preferable element size to be determined, and F_e is a flow-solution-variable over the element, like the pressure gradient or vorticity. In Eq. (9) we simply take the L^2 norm of the calculated variable. If the calculated solution is reasonably accurate, and the number of preferable elements is controlled by a ratio factor λ_r, we use

$$c = \lambda_r \frac{1}{N_e} \sum_e h_e \|F_e\|, \tag{10}$$

where h_e is the local element size for the mesh that is to be improved, N_e is the total number of elements in that mesh, and we sum over N_e.

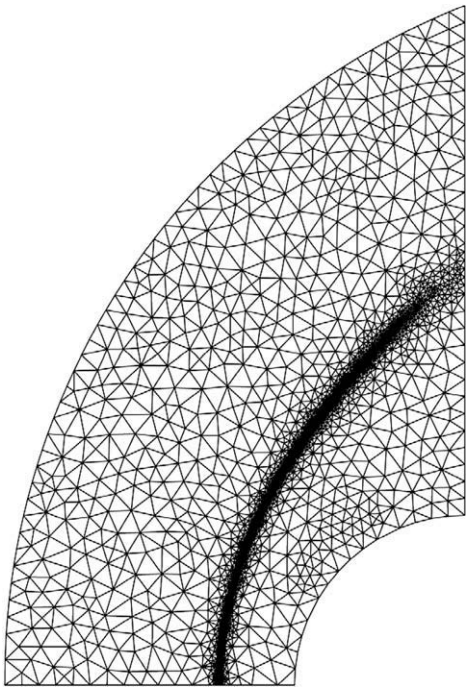

Fig. 3. Final mesh after six mesh adaptations for compressible flow passing a cylinder.

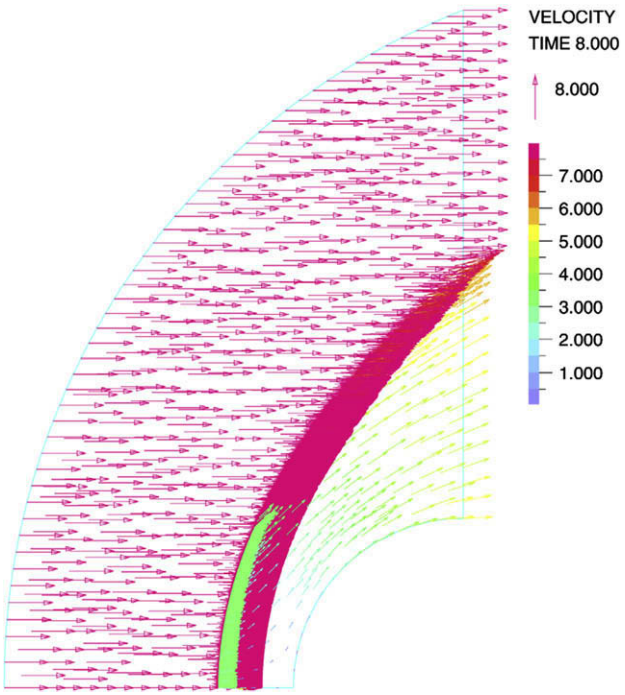

(a). Velocity.

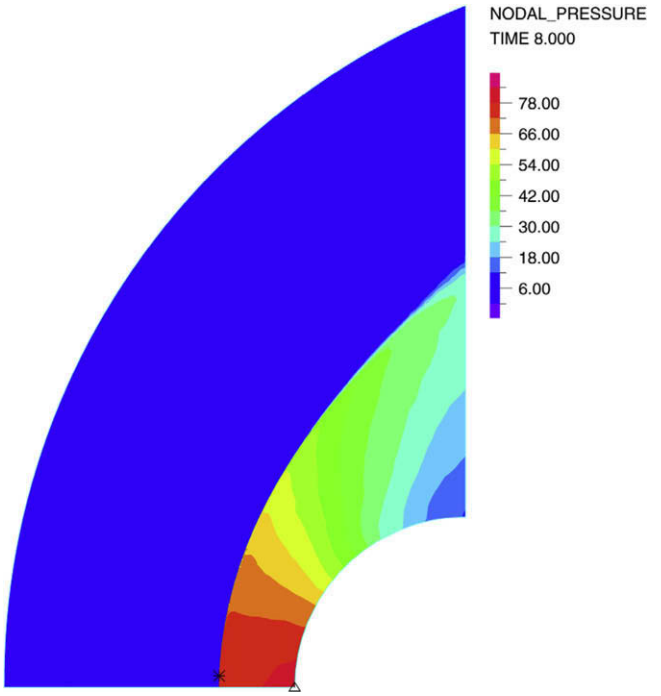

(b). Pressure.

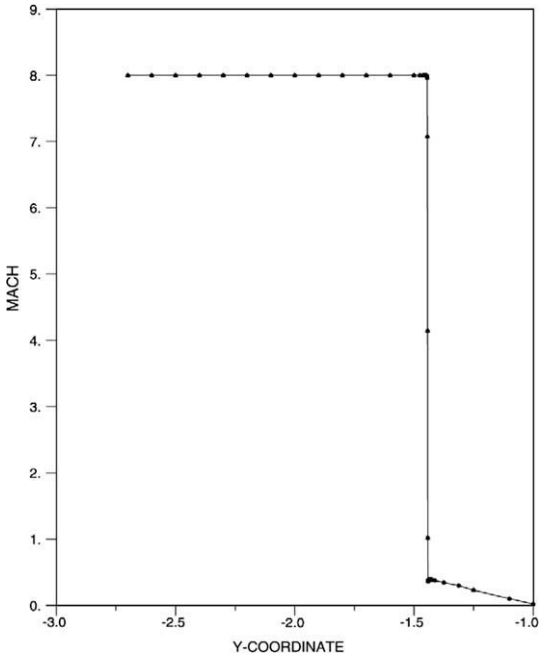

(c). Pressure along A–A.

Fig. 4. Calculated results using the final mesh.

In practice, elements of too large or too small sizes must be prevented, and hence limits on sizes must be specified. This results in the final formula for the preferable local element size

$$h_{ep} = \frac{c}{\max\left\{\min\left\{\|F_e\|, \frac{c}{h_{\min}}\right\}, \frac{c}{h_{\max}}\right\}}, \tag{11}$$

where $h_{\min}$ and $h_{\max}$ are, respectively, the minimum and maximum element sizes allowed in the mesh.

Eqs. (10) and (11) are used to generate triangular and tetrahedral elements with sides of (approximately) equal lengths, that is, geometrically isotropic elements. To generate anisotropic elements, the above approach can be used for the direction n (given by F_e) and then in the orthogonal directions we can obtain $h_{ep\tau}$ in a similar way

$$C(F_e^*): \quad h_{ep\tau}\|F_e^*\| = \lambda_\tau \frac{1}{N_e}\sum_e h_e\|F_e^*\|,$$

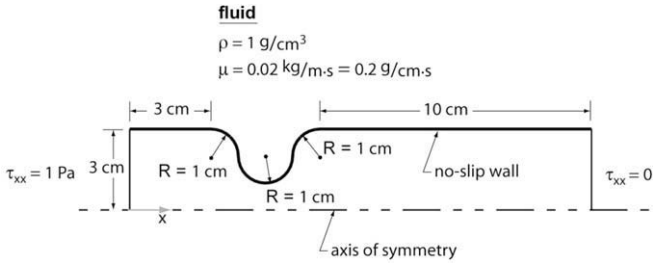

Fig. 5. Incompressible axisymmetric flow through a constriction.

where F_e^* can be the same as F_e or another flow-solution-variable over the element. For example, we can choose the second derivative $F_e^* = (I - nn) \cdot \nabla(h_e \| F_e \|)$.

The choice of F_e depends on the type of problem. For example, the pressure-gradient criterion $C\,(\nabla p_e)$ may be used for having a sufficient number of elements in areas where large pressure gradients are present. The vorticity criterion $C\,(\nabla \times \mathbf{v})$ may be used to improve the solution accuracy in boundary layers. In fact, any other solution variable or gradient can be used depending on the anticipated solution.

In practice, these criteria can be applied to the whole finite element model or only to certain element groups of the finite element model.

Then, each criterion produces a "to-be-repaired-element set" E of elements e associated with preferable element sizes h_{ep}

$$C(F_e) \to E\{e|h_{ep}\}. \tag{12}$$

Usually, one criterion is not sufficient to produce effective meshes. Therefore we allow certain operations on criteria to result in a combined set of elements to be repaired. The procedure works on each additional criterion as

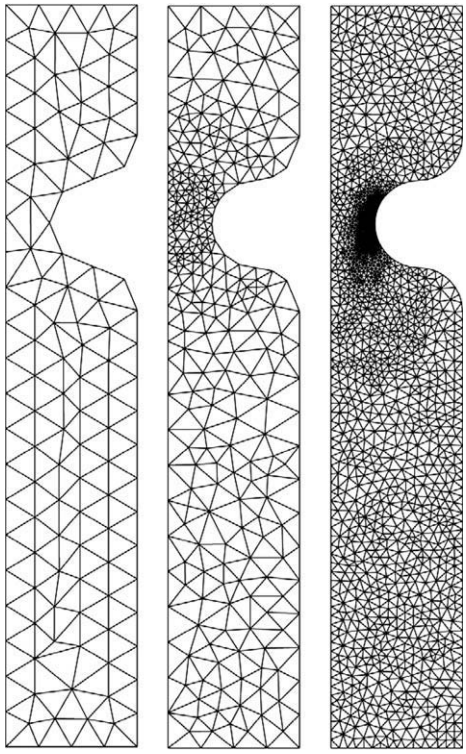

Fig. 6. The initial mesh and the two adaptively reached meshes.

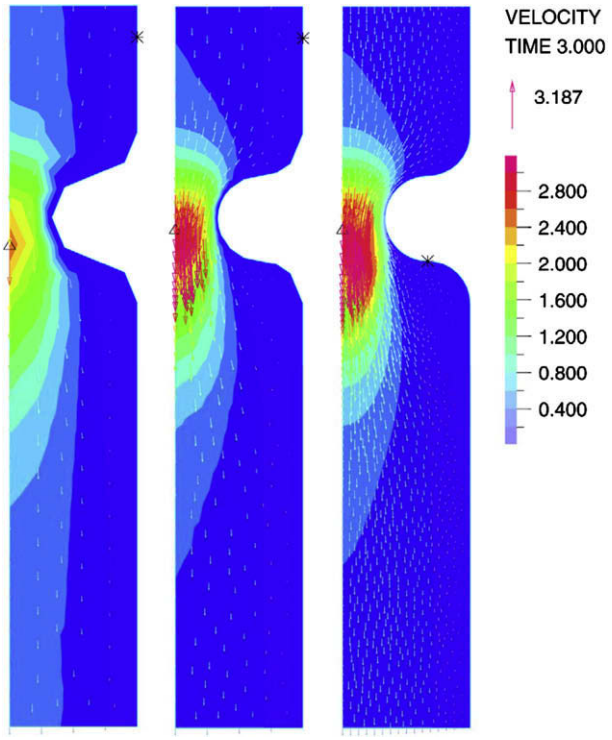

Fig. 7. Calculated velocity for flow through a constriction.

$$E = \emptyset$$
$$\text{for } i = 1, 2, \ldots \quad \{E =: \text{operation on } E \text{ and } E_i\}.$$

These operations are summarized in Table 1.

Finally, the preferable element sizes may be smoothed a few times using the iteration procedure

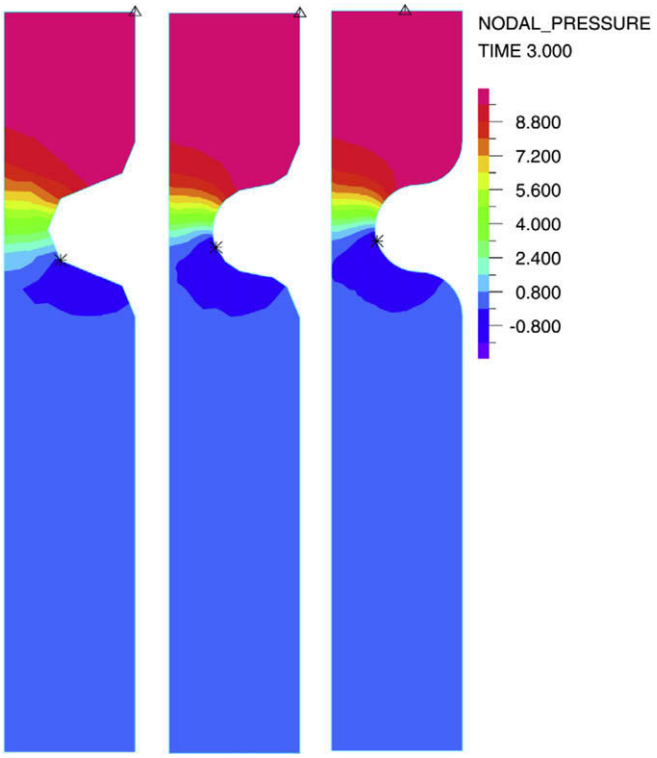

Fig. 8. Calculated pressure for flow through a constriction.

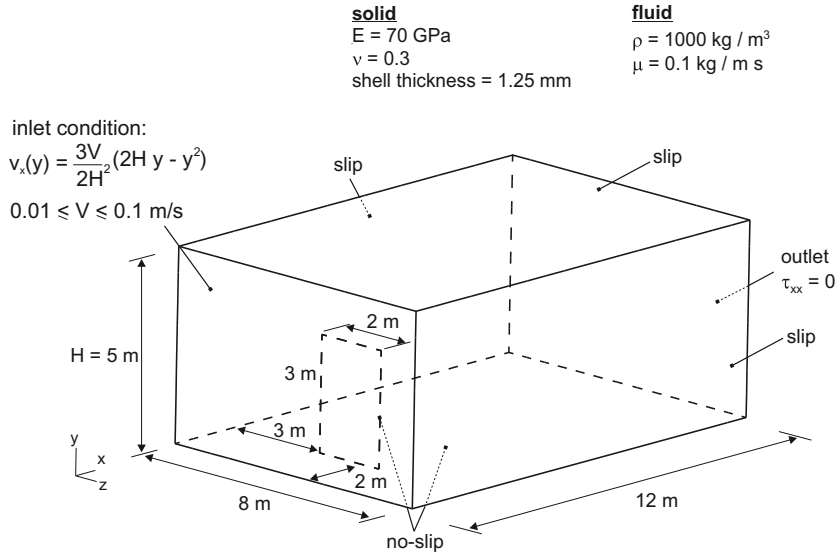

Fig. 9. Shell in steady-state cross-flow.

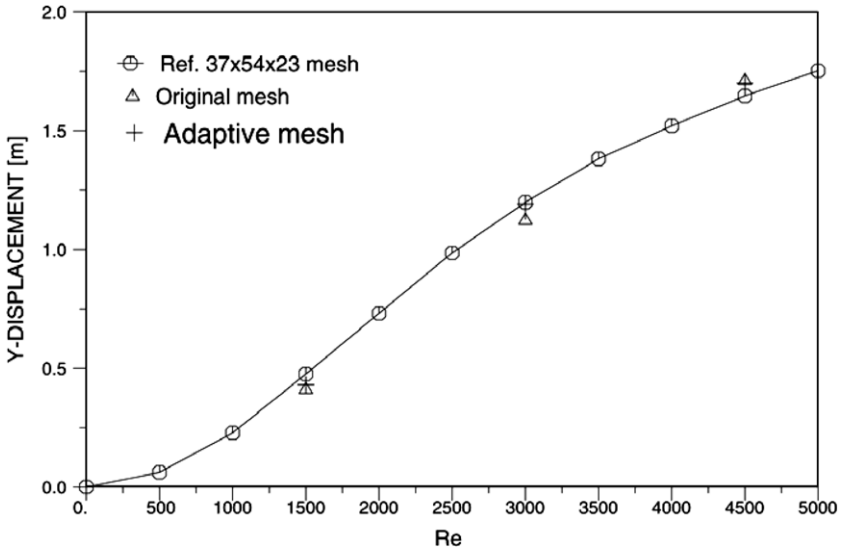

Fig. 10. Tip displacement of the shell in steady-state cross-flow (in the reference a uniform mesh of brick elements was used for the fluid).

$$h_{ep}^{k+1} = \frac{\sum_{nb} h_e h_{ep}^k}{\sum_{nb} h_e}; \quad k = 1, 2, \ldots, \tag{13}$$

where as indicated by "*nb*" the sum is carried out over the neighboring elements.

To reach the improved mesh with these flow-solution-variable criteria, we also use an algorithm to enable recovery of geometries independent of the element sizes. The recovery of geometry is based on spline interpolations used for the different parts of the complete geometry. This capability enables the algorithm to recover geometry when in practice during the finite element solution, the CAD geometry is no longer available or deformed, as encountered in FSI solutions.

5.2. Control on the maximum number of elements

The above element criteria basically re-scale element sizes to obtain a mesh in which the selected gradients times the element sizes are about constant and the geometry and boundary conditions are properly represented. In practice, the model size must be limited, that is, there must be an upper limit on the maximum number of elements allowed. When the total number of preferable elements N_{ep} is larger than the maximum number of elements allowed $N_{\max}$, we can increase the geometric size of all elements by a factor λ, that is, we change h_{ep} to λh_{ep}, with

$$\lambda = \max\left\{\left(\frac{N_{ep}}{N_{\max}}\right)^{\frac{1}{\sigma}}, 1\right\}, \tag{14}$$

where σ is the space dimension and

$$N_{ep} = \sum_e \frac{V_e}{V_{ep}} \tag{15}$$

with V_e the current element volume and V_{ep} the volume of the elements computed using the preferable element size.

Of course, depending on the meshing algorithm used, the final number of elements obtained after this adaptation could still be slightly larger or smaller than $N_{\max}$. The purpose of this scheme is to apply a limit on the size of the model.

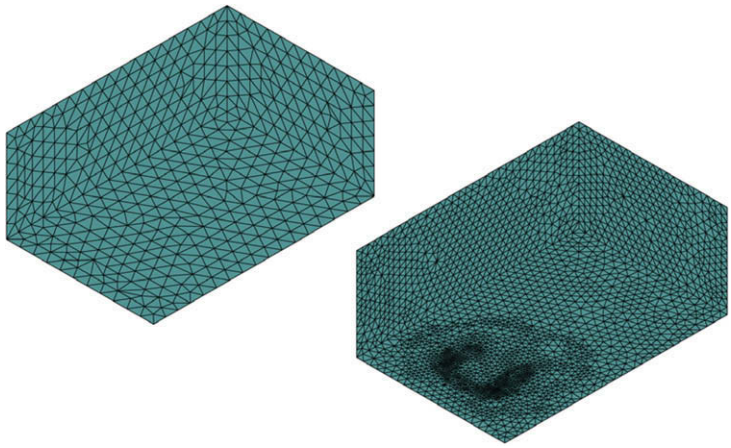

(a). View of complete domain (from below).

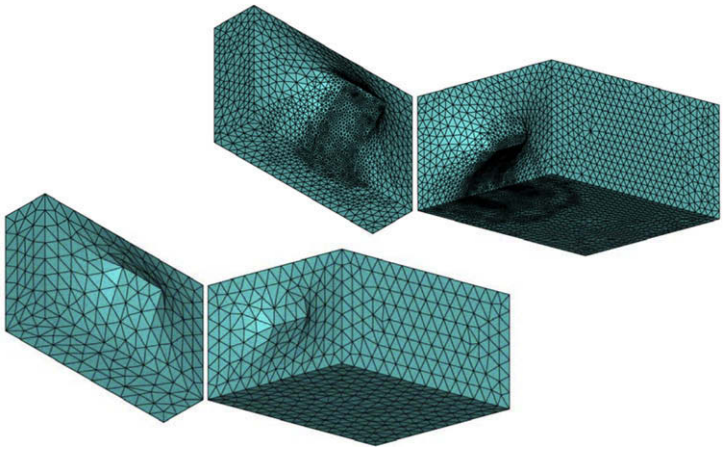

(b). Cross-sectional views at the plane of the cantilever shell (of the deformed meshes).

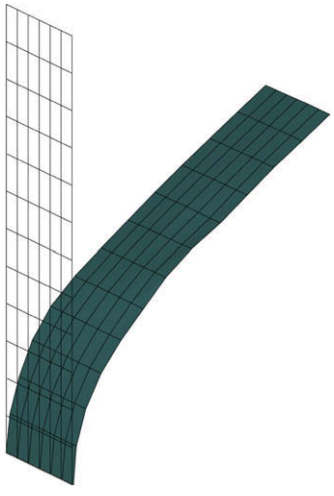

(c). Mesh of MITC4 shell elements, in original and final configurations (deformations are shown to scale).

Fig. 11. The starting CFD mesh, the final CFD mesh reached with three adaptations and the mesh of the shell, used in analysis of shell in cross-flow.

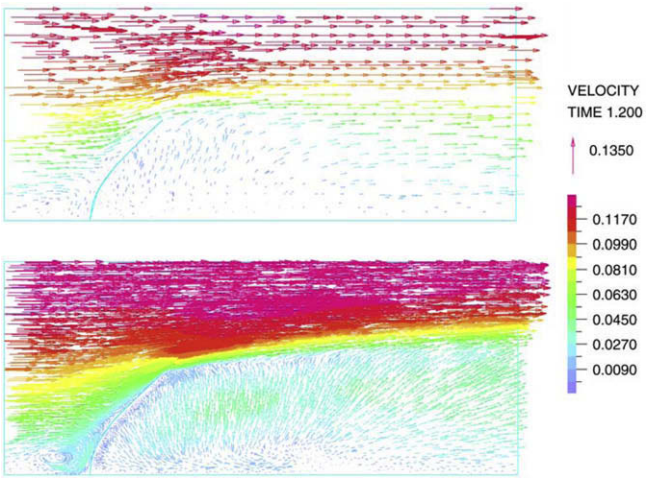

(a). Velocity.

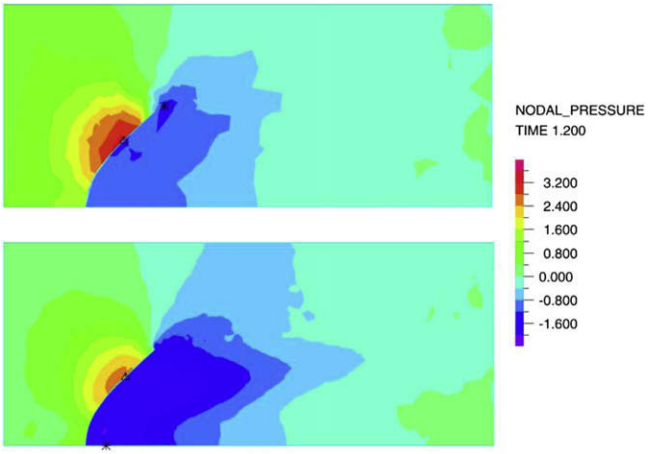

(b). Pressure.

Fig. 12. Calculated results in analysis of shell in cross flow for the starting mesh and the final mesh.

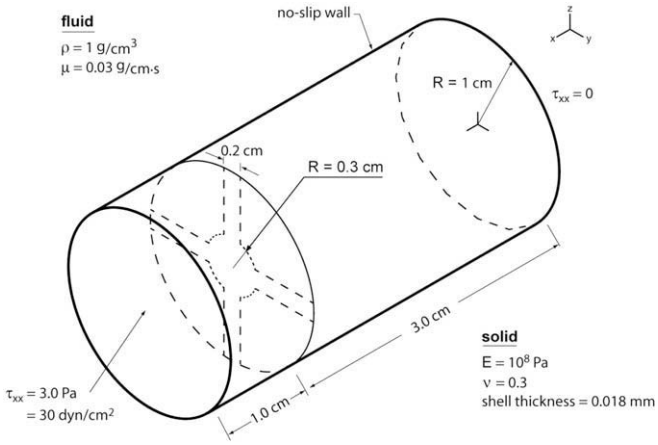

Fig. 13. Flow around blades.

5.3. Some additional considerations

The algorithms given above have been designed for the solution of problems where in pure CFD or in FSI solutions a chosen mesh does not yield sufficient accuracy, or even more severe, an FSI solution fails if a mesh adaption is not used because the fluid elements become too distorted.

In the solutions, the algorithms can be used at any time step. Appropriate element sizes are first estimated using C (F_e) and then the decision is made whether to adapt the mesh. If the mesh is to be adapted, the above criteria are employed to obtain the new mesh and the previous solution is mapped onto that mesh. This mapping includes also the mapping of the boundary conditions and material data. Of course, at this stage, the model could also be modified, for example in the boundary conditions and the constitutive data.

In the FSI solutions, we use the arbitrary-Lagrangian–Eulerian formulation for the fluid, previously described [4,8], to allow reasonable mesh deformations in each solution step, but once the mesh has been significantly distorted, a mesh adaptation is required. The mesh adaptation prevents too distorted elements and also distributes elements and element sizes such as to have an almost constant value for c in Eq. (9) for the fluid domain.

5.4. Overall strategies on obtaining adaptive solutions

While ideally, accurate steady-state and transient solutions could be obtained with the mesh adaptivity procedure, we have so far focused on the solution of steady-state problems. In principle, the above algorithms can also be used to solve transient problems, but in practice the error accumulation due to the changes in meshes over many time steps may be too large. The difficulty is that any error introduced at a particular time may be difficult to "iterate away" at a later time.

Considering steady-state pure CFD problems, a reasonably fine starting mesh is used that if needed is adapted by the above procedure, see Sections 6.1 and 6.2 for examples.

The solution of FSI problems can be much more challenging. A major difficulty arises when the required fluid element sizes are very small, as in boundary layers, and the structural deformations are rather large in an incremental step, measured on these fluid element sizes. In such cases, the fluid element mesh can become very distorted or, more severely, element overlapping may occur. Our strategy is, for such problems, to start the solution with a rather coarse finite element mesh and allow the large structural deformations to take place. Then, thereafter, the fineness of the fluid element mesh is increased. Since the structure will in this later phase only adjust its deformations by relatively small changes in geometry, required small fluid element sizes, as in boundary layers, can now be accommodated in the mesh adaptations to obtain the required solution accuracy.

In these adaptations of the mesh, we use the appropriate mesh criteria, including combinations as summarized in Table 1, and use the element size smoothing technique. An overriding criterion is the upper limit of the maximum number of elements that shall be used in the solution.

We should point out that in the mesh adaptivity scheme no actual error estimation is directly used. However, after a CFD mesh has been established that is deemed to be appropriate for an accurate solution, simple error indicators based on band plots can be used [27,28]. While not strict error estimates, these indicators are particularly attractive for the solid or structure in FSI solutions

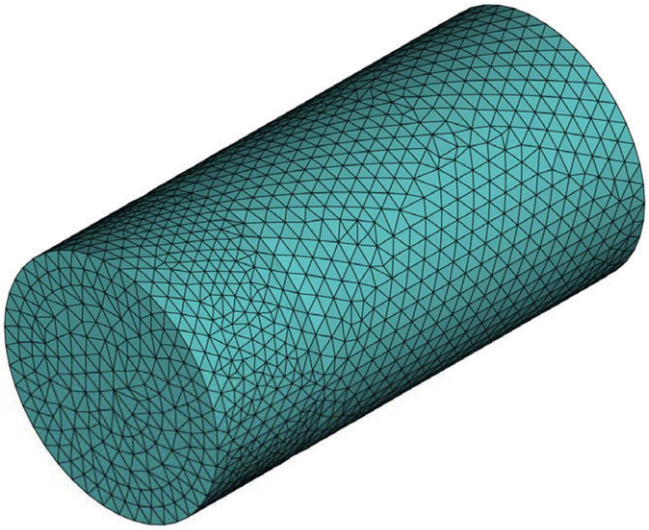

(a). CFD starting mesh.

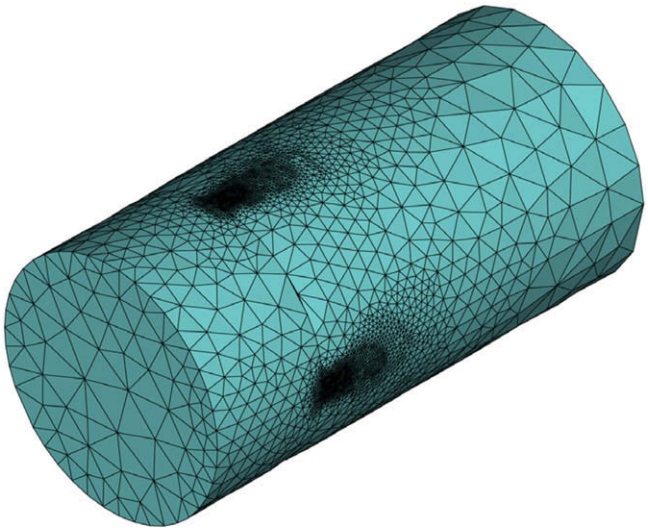

(b). CFD final mesh.

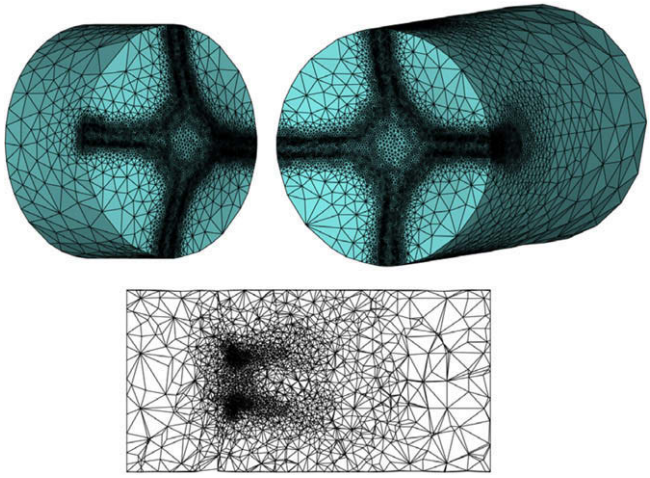

(c). CFD final mesh with cuts through domain.

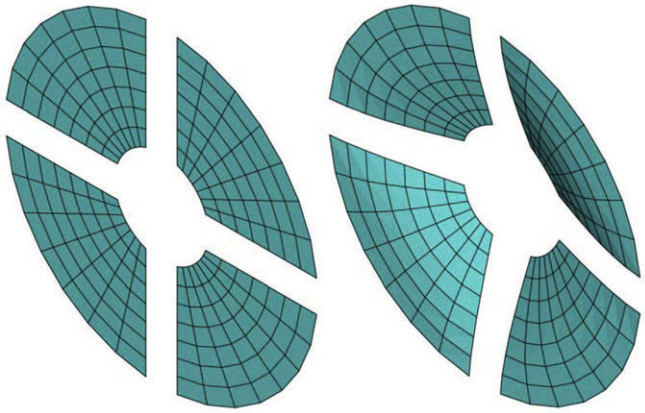

(d). Mesh of MITC4 shell elements, in original and final configurations (deformations are shown to scale).

Fig. 14. Meshes used for analysis of flow around blades.

[29]. If necessary the CFD mesh and the mesh of the solid could then be further refined.

6. Illustrative solutions

Our objective in this section is to present some illustrative solutions using the mesh adaptation techniques. In each case we give the criteria used, the starting and finally reached CFD meshes and the predicted solutions. In the FSI problems, the structure is represented by a reasonable mesh of shell or beam elements. For the incompressible flows, when the normal traction is specified, as at the inflow and outflow boundaries, we assume that the derivative of velocity with respect to the normal direction is zero. The remaining terms of the shear stress components are discretized and solved for.

The mesh adaptation procedure has been implemented in ADINA and we used this program to obtain all solutions.

6.1. Compressible flow passing a circular cylinder

We consider here the two-dimensional flow passing a circular cylinder with a free stream Mach number of 8. This problem has been solved by a number of authors to benchmark solution schemes, see, e.g. Ref. [30]. The problem is described in Fig. 1. Using symmetry conditions and the supersonic characteristics, only the domain shown in Fig. 2 is modeled.

Fig. 2 gives the starting mesh of 1758 elements for the analysis. The flow-solution-variable used here is the pressure gradient, and we use $(h_{\min}, h_{\max}, \lambda_r) = (2 \times 10^{-4}, 0.2, 1)$ to first adapt the mesh, and gradually modify these data to $(h_{\min}, h_{\max}, \lambda_r) = (10^{-7}, 0.1, 0.5)$ for the last choice of mesh. The key aspect in this analysis is to accurately predict the shock front in the flow.

For the analysis, six mesh adaptations were used to reach the final mesh of 56,471 elements given in Fig. 3. The computed solutions of velocity, pressure as well as Mach number are given in Fig. 4. The solutions are very accurate.

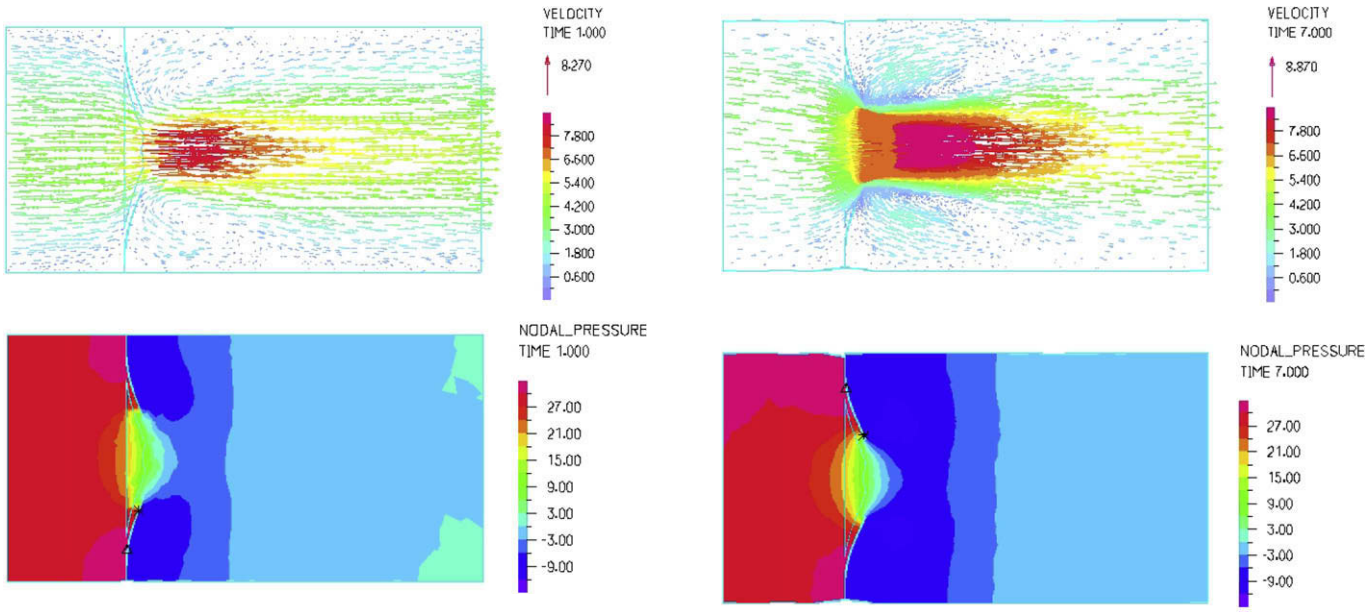

(a). Results using starting mesh.

(b). Results using final mesh.

Fig. 15. Calculated results on center plane in analysis of flow around blades.

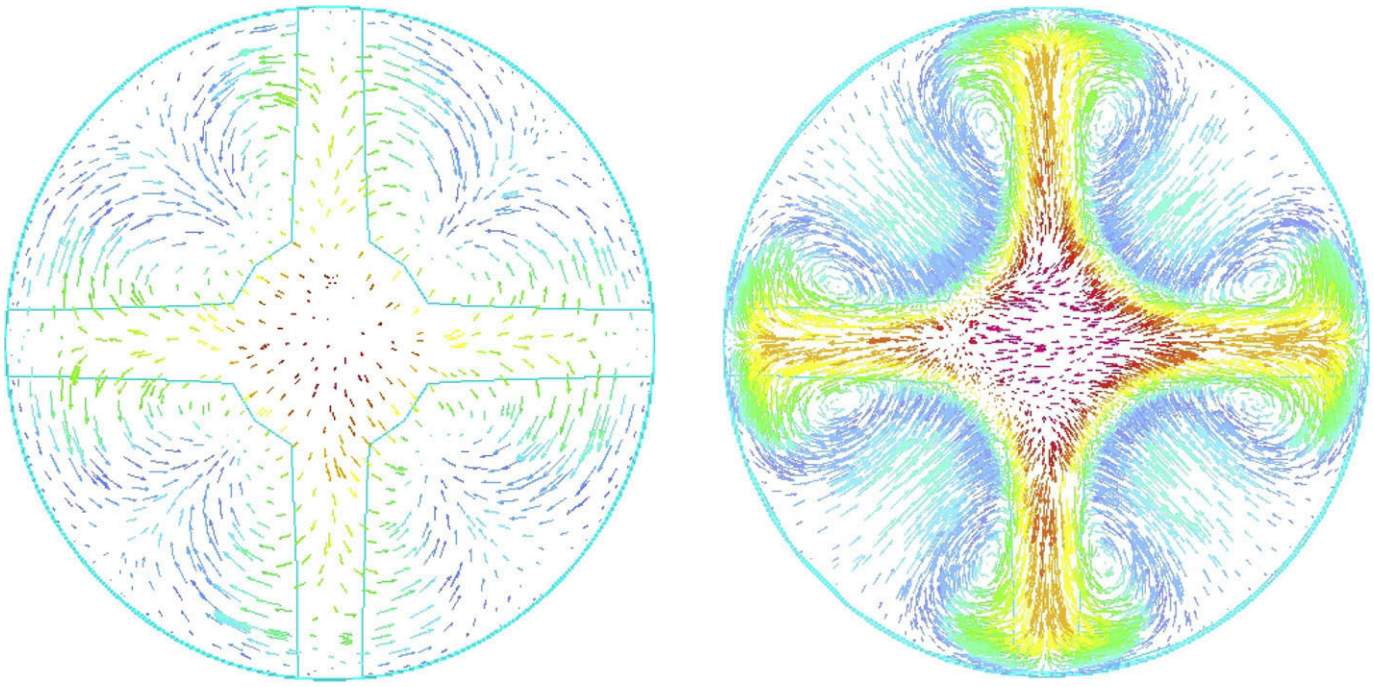

(a). Results using starting mesh.

(b). Results using final mesh.

Fig. 16. Velocities on plane 0.5 cm downstream from the blades.

6.2. Incompressible axisymmetric flow through a constriction

The problem is described in Fig. 5. The objective in this analysis is to predict accurately the flow and pressure drop across the constriction.

In this solution, the mesh was adapted 2 times. To obtain the second mesh, the criterion of combined pressure gradient and vorticity was used, with the data for each criterion $(h_{\min}, h_{\max}, \lambda_r) = (0.01, 0.5, 1.2)$. To obtain the third mesh, we only used the vorticity criterion with $(h_{\min}, h_{\max}, \lambda_r) = (0.01, 0.2, 0.7)$ in order to enhance the mesh to be favourable for vorticity and boundary-layer results.

Fig. 6 shows the starting mesh of 198 elements. This mesh does not accurately represent the circular boundary. Fig. 6 also gives the final mesh of 3784 elements where it is noted that the geometry of

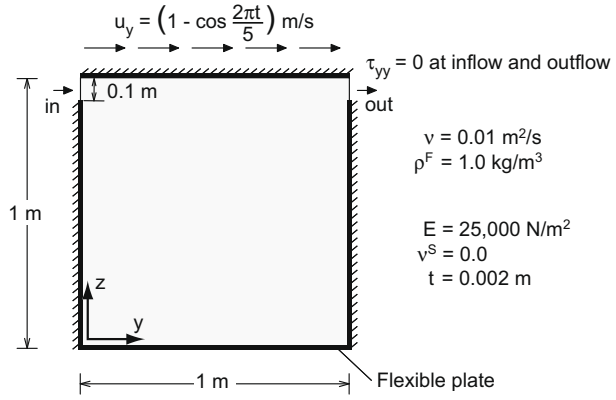

Fig. 17. Driven open-cavity on flexible plate.

the constriction is now accurately captured. This geometry was retrieved from the starting mesh without recourse to the actual geometry lines.

The calculated solutions are given in Figs. 7 and 8 for all three meshes.

6.3. Shell in steady-state cross-flow

This FSI problem, described in Fig. 9, was already considered in Ref. [23]. Fig. 10 gives the solution reported in Ref. [23] using $37 \times 54 \times 23$ brick elements for various Reynolds numbers, and the solutions obtained with the adaptive mesh procedure for three Reynolds numbers. In terms of number of elements used, the mesh of brick elements must of course be expected to be more effective than a free-form mesh of tetrahedral elements. In these solutions, we used the combined pressure gradient and vorticity criterion. In each of the three analyses, we used for the selection of the second mesh $(h_{\min}, h_{\max}, \lambda_r) = (0.01, 0.7, 1)$ and for the calculation of the third and fourth meshes (0.01,0.3,0.5). We see that, considering the tip displacement of the cantilever, the starting mesh solutions compare already reasonably well with the results published in Ref. [23], but the adaptively reached fine mesh solutions are closer.

In all three cases, the number of elements in the initial mesh was around 15,000, and the number of elements in the final meshes was around 330,000. Fig. 11 gives the starting mesh and the final mesh reached for the case of Re = 4500. In particular, the fluid mesh near the solid shell is shown in Fig. 11b to indicate the mesh complexity that can occur. Finally, the calculated results on the longitudinal cutting center plane are shown in Fig. 12. Here the velocity and pressure fields calculated with the starting and final meshes show expected differences.

6.4. Flow around blades

Fig. 13 describes this FSI problem. To obtain an accurate solution, a fairly fine mesh needs to be used near the blades, but away from the blades a coarser mesh can be employed. Here we used the combined criterion of pressure gradient and vorticity with $(h_{\min}, h_{\max}, \lambda_r) = (0.1, 0.5, 1)$ to (0.01,0.2,0.8) in six mesh adaptations. The number of elements was initially 34,041 and gradually reached 547,741 in the final mesh.

To solve this problem, symmetry conditions could be used to reduce the size of the model. However, we deliberately did not use symmetry conditions in order to have a more complete testing of our mesh adaptivity schemes.

Fig. 14 shows the starting (coarse) mesh and the fine mesh reached adaptively. Fig. 15 shows the velocity and pressure fields on the center longitudinal cutting plane and Fig. 16 gives the velocity fields on a vertical cross-section 0.5 cm downstream from the blades, as calculated using the starting mesh and the final mesh. We notice that the predicted flow is virtually symmetric. We also notice that, with the increased number of elements near the blades, the secondary flows are well captured.

6.5. Driven open-cavity on membrane

The problem is described in Fig. 17. Almost the same problem is solved in Ref. [31] but we use a stiffer plate material (the Young's

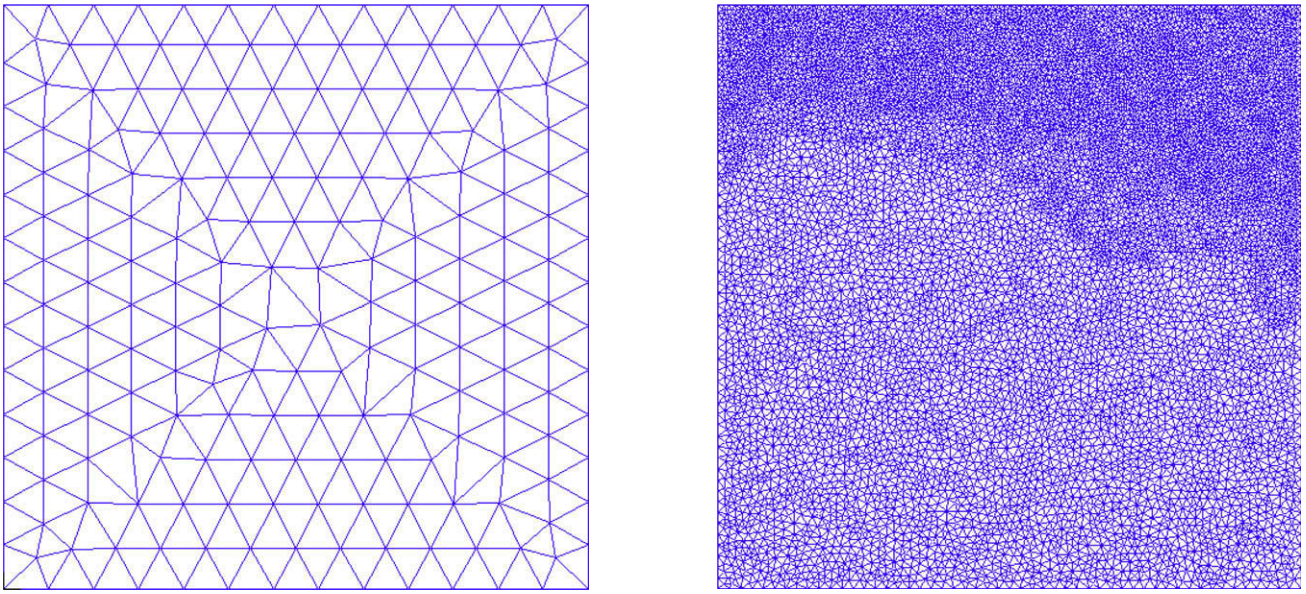

(a). Starting CFD mesh.

(b). Final CFD mesh.

Fig. 18. CFD meshes used for open-cavity on flexible plate.

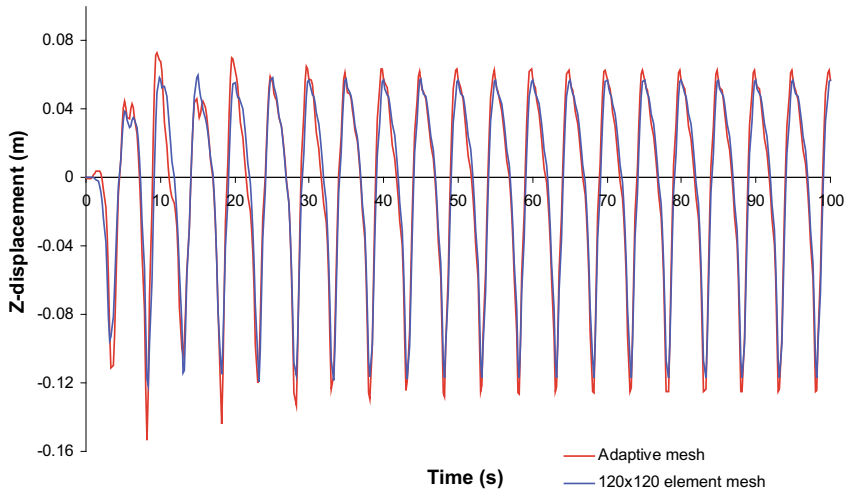

Fig. 19. Vertical displacement at mid-point of flexible plate in driven open cavity problem (the adaptive FCBI solution used the steady-state solution as initial condition).

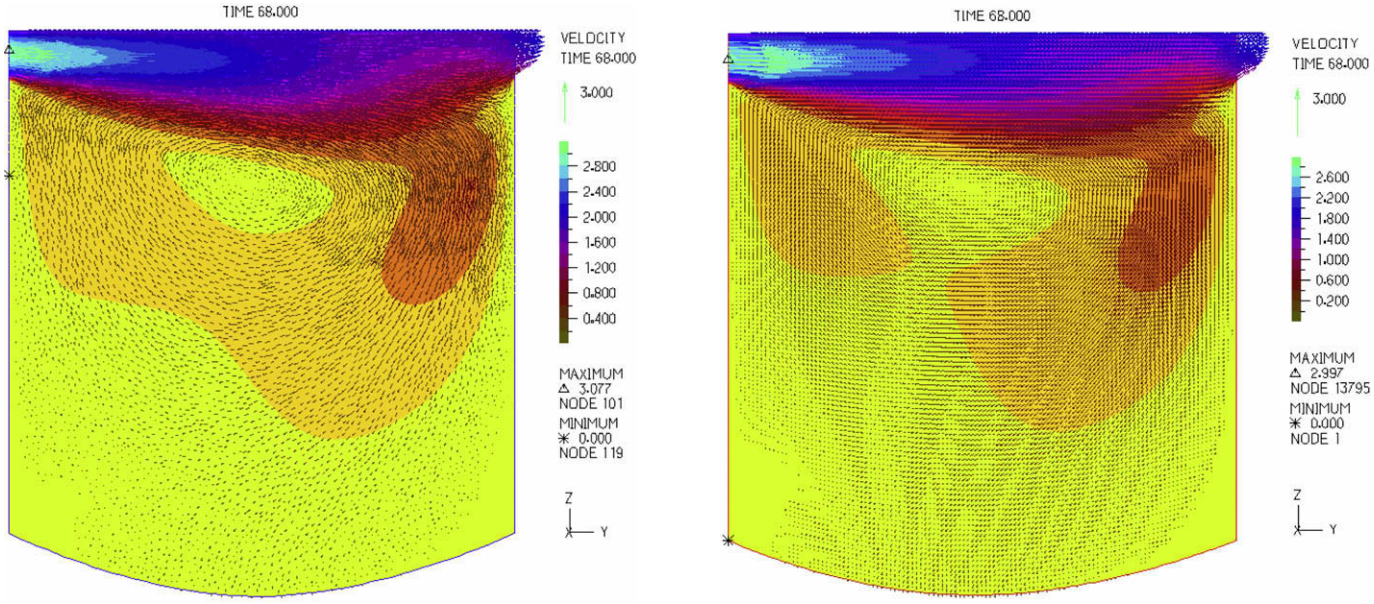

(a). Results using adaptively reached mesh.

(b). Results using uniform mesh.

Fig. 20. Computed velocities at time 68 using the adaptively reached mesh and the uniform mesh of 120 × 120 square 4-node FCBI elements.

modulus is 100 times larger but still orders of magnitude smaller than even for a typical rubber material). The plate is modeled using 120 equal-size 2-node isoparametric beam elements [10].

This is a transient analysis, and for transient analyses, fully adaptive solutions during the time integrations are (still) computationally too expensive and would accumulate significant solution errors. Therefore, we first solved for the steady-state response with the maximum velocity-loading, equal to 1. Fig. 18 shows the meshes. The final mesh reached in two adaptations using the combined criterion of pressure gradient and vorticity with $(h_{\min}, h_{\max}, \lambda_r) = (0.01, 0.5, 0.6)$ contains 19,536 elements, with the smallest and largest elements of sizes equal to 3.5 mm and 21.2 mm, respectively. We then used this refined mesh for the transient solution with the time integration scheme of Ref. [22], for the fluid and the solid, and the time step = 0.1 s.

Fig. 19 gives the transient response of the bottom membrane. We note that the mean displacement of the plate is downward and the plate oscillates about that mean displacement.[1] After a short transient, the response repeats itself but we ran the solution over a larger time span merely because a larger time span was used in Ref. [31] to identify instabilities in FSI algorithms. The calculated response is compared with the response obtained using a uniformly fine mesh of 120 × 120 4-node FCBI elements. Figs. 20 and 21 give the velocities and pressures at time 68. We see that the solutions calculated with the adaptively reached mesh are close to those

[1] In our solution, the bottom plate moves in the mean downwards whereas in Ref. [31], and the references given therein, the membrane moves upwards. This difference is likely due to how we model the physical inlet and outlet boundary conditions (see Section 6).

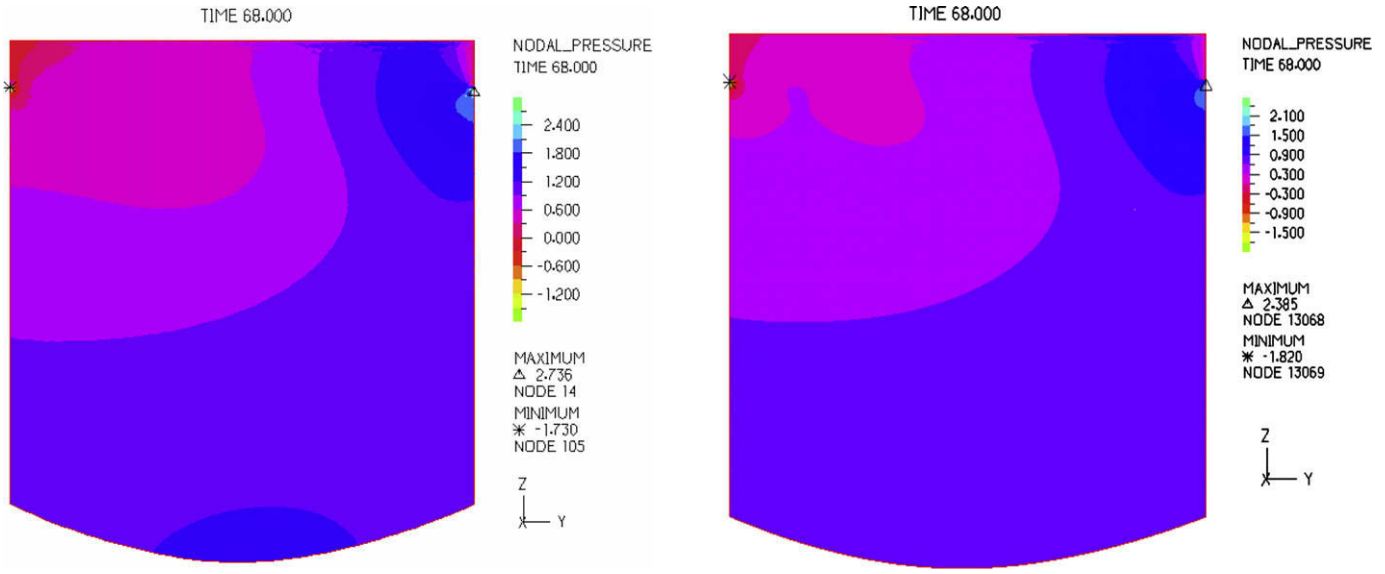

(a). Results using adaptively reached mesh.

(b). Results using uniform mesh.

Fig. 21. Computed pressure at time 68 using the adaptively reached mesh and the uniform mesh of 120 × 120 square 4-node FCBI elements.

obtained with the uniform mesh of 14,400 elements. However, the 4-node quadrilateral elements in a uniform mesh are more powerful and a smaller number of elements results in an acceptable solution.

7. Concluding remarks

The objective in this paper was to present a procedure for the adaptive repair, coarsening and refining of meshes used in the simulation of fluid flows. The procedure can be used in pure CFD solutions and in fluid-structure interaction analyses using an arbitrary-Lagrangian–Eulerian formulation.

The two key aspects of the procedure are that, firstly, rather coarse starting meshes are employed and, secondly, various simple criteria are used for the mesh adaptation. The use of an initial coarse mesh can be important in FSI solutions in order to avoid large element distortions. The use of the simple criteria is effective because exact error measures are still out of reach, and various criteria can be combined to steer the selection of improved meshes. It is also easy to add a new criterion that based on further research may be useful.

While the procedure can already be used quite effectively to solve complex CFD and FSI problems, various improvements would be very valuable. These pertain, for example, to the use of more effective criteria, ideally actual error measures, the use of more powerful CFD elements and meshes in which the elements are better aligned with the fluid flow, and also adaptive re-meshing of the structures. Hence, there is still much further development to be accomplished. However, the procedure given in the paper provides a powerful basis on which we can build our further developments.

Acknowledgements

We would like to thank Drs. Shanhong Ji and N. Elabbasi for their help in some of the example solutions.

References

[1] Bathe KJ, editor. Proceedings of the fourth M.I.T. conference on computational fluid and solid mechanics. Elsevier Science; 2007.
[2] Wang X. Fluid–solid interaction. Elsevier Science; 2008.
[3] Rugonyi S, Bathe KJ. On finite element analysis of fluid flows fully coupled with structural interactions. Comput Model Eng Sci 2001;2:195–212.
[4] Bathe KJ, Zhang H. Finite element developments for general fluid flows with structural interactions. Int J Numer Meth Eng 2004;60:213–32.
[5] Wang X, Bathe KJ. Displacement/pressure based mixed finite element formulations for acoustic fluid–structure interaction problems. Int J Numer Meth Eng 1997;40:2001–17.
[6] Bathe KJ, Nitikitpaiboon C, Wang X. A mixed displacement-based finite element formulation for acoustic fluid–structure interaction. Comput Struct 1995;56(2/3):225–37.
[7] Nitikitpaiboon C, Bathe KJ. An arbitrary Lagrangian–Eulerian velocity potential formulation for fluid–structure interaction. Comput Struct 1993;47:871–91.
[8] Bathe KJ, Zhang H, Wang MH. Finite element analysis of incompressible and compressible fluid flows with free surfaces and structural interactions. Comput Struct 1995;56:193–213.
[9] Bathe KJ, Zhang H, Ji S. Finite element analysis of fluid flows fully coupled with structural interactions. Comput Struct 1999;72:1–3. 1-16.
[10] Bathe KJ. Finite element procedures. Prentice-Hall; 1996.
[11] Bathe KJ, Zhang H. A flow-condition-based interpolation finite element procedure for incompressible fluid flows. Comput Struct 2002;80:1267–77.
[12] Eterovic AL, Bathe KJ. On the treatment of inequality constraints arising from contact conditions in finite element analysis. Comput Struct 1991;40(2):203–9.
[13] El-Abbasi N, Bathe KJ. Stability and patch test performance of contact discretizations and a new solution algorithm. Comput Struct 2001;79:1473–86.
[14] Rugonyi S, Bathe KJ. An evaluation of the Lyapunov characteristic exponent of chaotic continuous systems. Int J Numer Meth Eng 2003;56:145–63.
[15] Bathe KJ. The inf–sup condition and its evaluation for mixed finite element methods. Comput Struct 2001;79:243–52, 971.
[16] Kohno H, Bathe KJ. A flow-condition-based interpolation finite element procedure for triangular grids. Int J Numer Meth Fluids 2006;51:673–99.
[17] Banijamali B, Bathe KJ. The CIP method embedded in finite element discretizations of incompressible flows. Int J Numer Meth Eng 2007;71:66–80.
[18] Iannelli J. Characteristics finite element methods in computational fluid dynamics. Springer-Verlag; 2006.
[19] Glaister P. An approximate linearized Riemann solver for the three-dimensional Euler equations for real gases using operator splitting. J Comput Phys 1988;77:361–83.
[20] Chapelle D, Bathe KJ. Fundamental considerations for the finite element analysis of shell structures. Comput Struct 1998;66:19–36.
[21] Chapelle D, Bathe KJ. The finite element analysis of shells – fundamentals. Springer-Verlag; 2003.
[22] Bathe KJ. Conserving energy and momentum in nonlinear dynamics: a simple implicit time integration scheme. Comput Struct 2007;85:437–45.
[23] Bathe KJ, Ledezma GA. Benchmark problems for incompressible fluid flows with structural interactions. Comput Struct 2007;85:628–44.
[24] Degroote J, Bathe KJ, Vierendeels J. Performance of a new partitioned procedure versus a monolithic procedure in fluid–structure interaction. Comput Struct 2009;87:793–801.

[25] Ainsworth M, Oden JT. A posteriori error estimation in finite element analysis. New York: J. Wiley; 2000.
[26] Grätsch T, Bathe KJ. A posteriori error estimation techniques in practical finite element analysis. Comput Struct 2005;83:235–65.
[27] Sussman T, Bathe KJ. Studies of finite element procedures – on mesh selection. Comput Struct 1985;21:257–64.
[28] Sussman T, Bathe KJ. Studies of finite element procedures – stress band plots and the evaluation of finite element meshes. J Eng Comput 1986;3(3): 178–91.
[29] Bathe KJ. The finite element method. In: Wah B (Ed.). Chapter in encyclopedia of computer science and engineering. J. Wiley and Sons; 2009. p. 1253–64.
[30] Osher S, Chakravarthy S. Upwind schemes and boundary conditions with applications to Euler equations in general geometries. J Comput Phys 1983;50:447–81.
[31] Küttler U, Wall W. Fixed-point fluid–structure interaction solvers with dynamic relaxation. Comput Mech 2008;43:61–72.